Electronic Supplementary Material (ESI) for ChemComm.

Semi-crystalline carbonaceous structure as a wide-spectrum-responsive photocatalyst for efficient redox catalysis

Pengju Yang,*[a] Ruonan Wang,[a] Hongxia Zhang, *[a] Jianghong Zhao,[a] Peng Wang,[c] Hu Shi*[b] and Hengquan Yang*[a]

[a] School of Chemistry and Chemical Engineering, Shanxi University, Taiyuan 030006, China

[b] School of Chemistry and Chemical Engineering, & Institute of Molecular Science, Shanxi University, Taiyuan 030006, China

[c] School of Material and Chemical Engineering, Xuzhou Institute of Technology, Xuzhou 221018, China

Sample Preparation: Firstly, 0.24 g dicyandiamide and 0.24 g p-phenylenediamine were dissolved in 60 mL water and stirred well. And then, the above mixture solution was sealed into a Teflon-lined stainless steel autoclave. Finally, the reaction was maintained at different temperature (140 °C, 160 °C, 180 °C and 200 °C) for 10 h and then cooled to room temperature naturally. The collected mixture was subjected to high-speed centrifugation at 8000 rpm for 30 min to obtain sample. The samples prepared at 140 °C, 160 °C, 180 °C and 200 °C were denoted as ONCS-140, ONCS-160, ONCS-180 and ONCS-200, respectively.

Characterization: X-ray powder diffraction patterns of all samples were performed on a D8 Advance Bruker X-ray diffractometer. Transmission electron microscopy (TEM) of all samples were analyzed by a JEOL microscope (JEM-2010). Raman spectra were recorded on a LABRAM-HR in plus laser Raman spectrometer. Fourier transform infrared spectroscopy was analyzed on a Nicolet Magna-IR 550-II spectrometer. UV-Visible absorption spectroscopy was analyzed using a Shimadzu UV-3600 UV-Vis-NIR spectrophotometer. Photoluminescence spectra of all samples were measured by a FL spectrophotometer (FLSP920). Electron paramagnetic resonance was analyzed on a Bruker model A300 spectrometer. X-ray photoelectron spectroscopy (XPS) results were obtained on an XPS spectrometer (Thermo ESCALAB 250, C1s of 284.6 eV was used as reference). The N_2 adsorption/desorption of all samples were measured by a Tristar-3000 apparatus at 77 K. Hall Effect was analyzed on a Hall effect measurement system (Joule Yacht, HET-RT). Electrochemical measurements were conducted with a BAS Epsilon Electrochemical System in a conventional three electrode cell (Pt sheet as the counter electrode; saturated calomel electrode as the reference electrode). The working electrode was prepared by dip-coating photocatalyst slurry on ITO glass. Infrared (IR) thermal images and temperature change were recorded by a thermal imaging camera (Ti480, Fluke). In order to uncover the functional groups changes and/or atoms doping, the theoretical calculations were performed by a suit of Gaussian software (Gaussian 09; Revision D.01; M. J. Frisch, et al.). The b3lyp/6-31g* was used to obtain the LUMO-HOMO data.

Photocatalytic test: Photocatalytic hydrogen evolution reactions were performed using a closed reaction system. In brief, 2 mg photocatalyst was added into 19 mL water/formic acid (18.5:0.5) solution and stirred well. Then, the reaction bottle was evacuated to eliminate air before reaction and

then the reaction system was full of Ar gas to reach a pressure of 1 atm. The reaction temperature was maintained at 30 ℃. The produced hydrogen was analyzed by a gas chromatography (Agilent 7820A). 50 W LED lamps (530 nm, 660 nm, 730 nm and 800 nm) were employed as light source. Cocatalyst Pt was loaded by an in-situ photo-deposition approach using H_2PtCl_6 as precursor.

Photocatalytic benzyl alcohol oxidation reactions were carried out using a small reaction bottle. Photocatalyst (2 mg) was poured into the mixture solution with 0.05 mmol benzyl alcohol dissolved in the benzotrifluoride (3 mL). The mixture was transferred into a 10 mL Pryex glass bottle filled with pure oxygen (1 atm) and irradiated for 24 h by 50 W LED lamps (530 nm, 660 nm, 730 nm and 800 nm). The temperature of the reactions was maintained at 60 °C. The products were analyzed by gas chromatograph (FID detector).

QY Measurement: The QY for hydrogen evolution was measured by using monochromatic LED lamp with band-pass filter as excitation light. The irradiation area was 0.196 cm^2. The light intensity values of 450, 530, 610, 660, 730 and 800 nm were 22.3, 22.1, 22.2, 22.2, 22.3 and 22.2 mW cm^{-2}, respectively (ILT 950 spectroradiometer). The QY was calculated as QY=Ne/Np*100%=2M NAhc/SPtλ*100% (M: the H_2 amount, NA: Avogadro constant, h: Planck constant, c: light speed, S: irradiation area, P: light intensity, t: reaction time, λ: the wavelength of light).

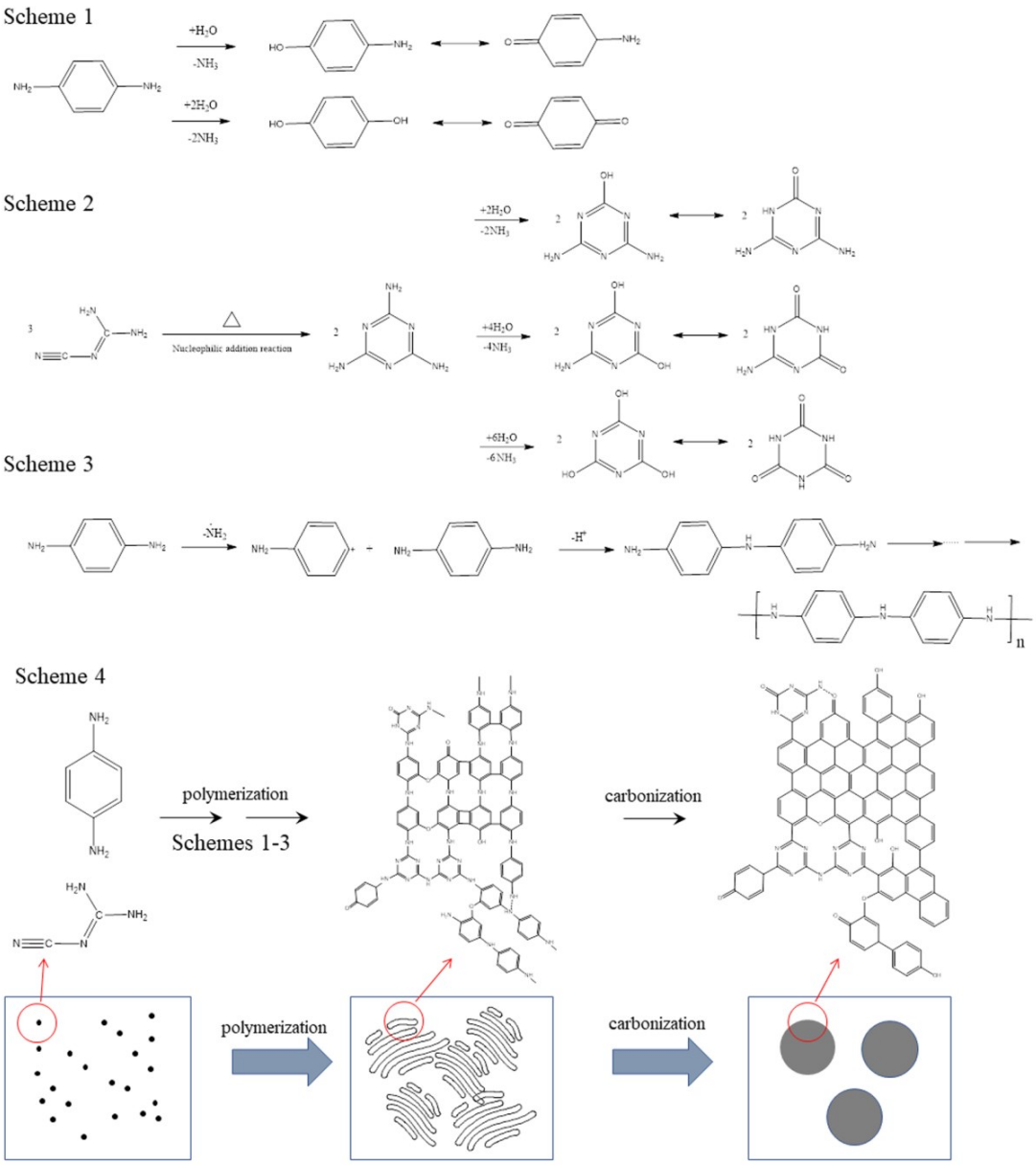

Figure S1. Illustration of the ONCS synthesis by a hydrothermal method.

Generally, hydrothermal reactions are carried out in aqueous media at high pressure and high temperature. As known, water in subcritical condition acts differently compared to water at ambient condition. The unique characteristic of the subcritical water is the ionization constant. The high range of ionization constant is indicating a high amount of H^+ and OH^- ions in the subcritical conditions. In principle, the high concentration of H^+ and OH^- ions provides the possibility for acid- or base-catalyzed reactions.

In the present work, dicyandiamide and p-phenylenediamine were used as precursors for preparing ONCS. Under hydrothermal processes (high concentration of H^+ and OH^- ions), p-Aminophenol and hydroquinone can be formed via hydrolysis of p-phenylenediamine (Scheme 1). Moreover, under high temperature conditions, dicyandiamide molecules can react with each other to form melamine by a nucleophilic addition reaction (Scheme 2). At the same time, ammeline, am elide and cyan uric acid will be formed via hydrolysis of melamine under acid/base conditions (subcritical water provides high

concentration of H^+ and OH^- ions) (Scheme 2).

In principle, under high temperature conditions, p-phenylenediamine probably can be decomposed into NH_2-radical and p-aminophenyl carbocation. And then, the p-aminophenyl carbocation can attack other p-phenylenediamine molecules to form 4, 4'-diaminodiphenylamine, and even form polyaniline by a series of radical reactions (Scheme 3). Especially, during the polymerization processes of p-phenylenediamine, the melamine and hydrolysis products (Schemes 1-2) will inevitably participate in the polymerization reaction, thus inducing oxygen species into the polymer analogue (Scheme 4). Finally, the formed polymer analogue can be carbonized into ONCS under high pressure and high temperature conditions (Scheme 4). The possible formation process of ONCS is shown in Figure S1.

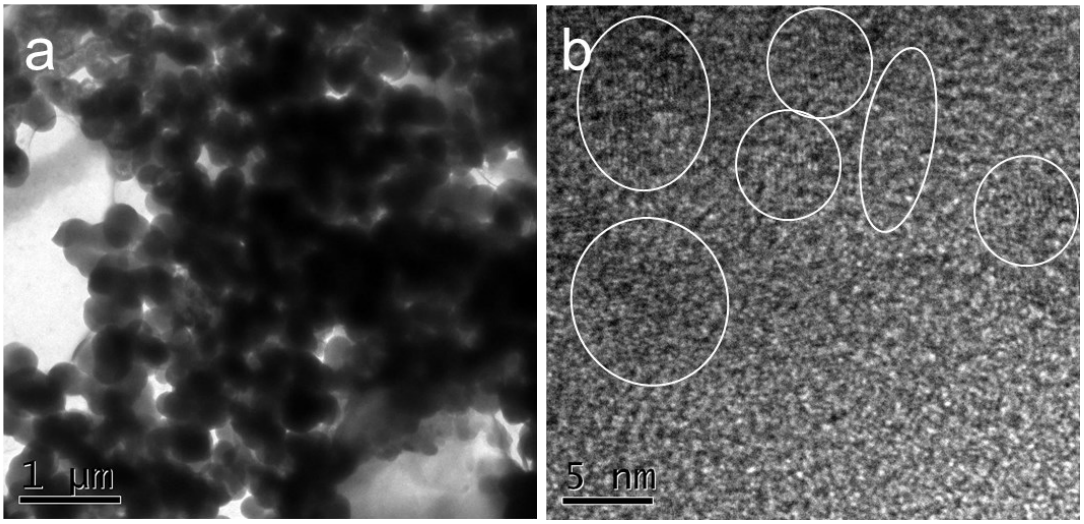

Figure S2. TEM and HRTEM images of ONCS-160.

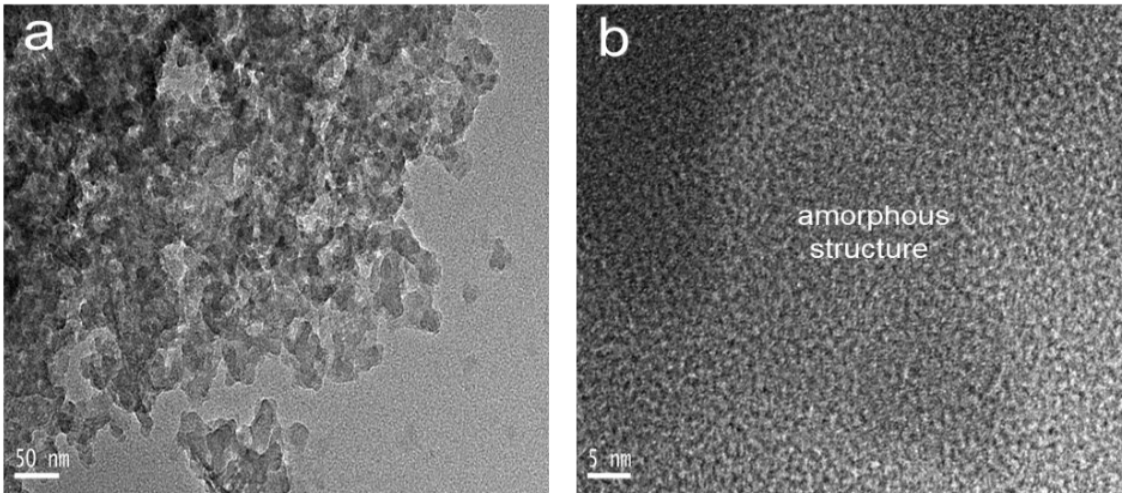

Figure S3. TEM and HRTEM images of ONCS-140.

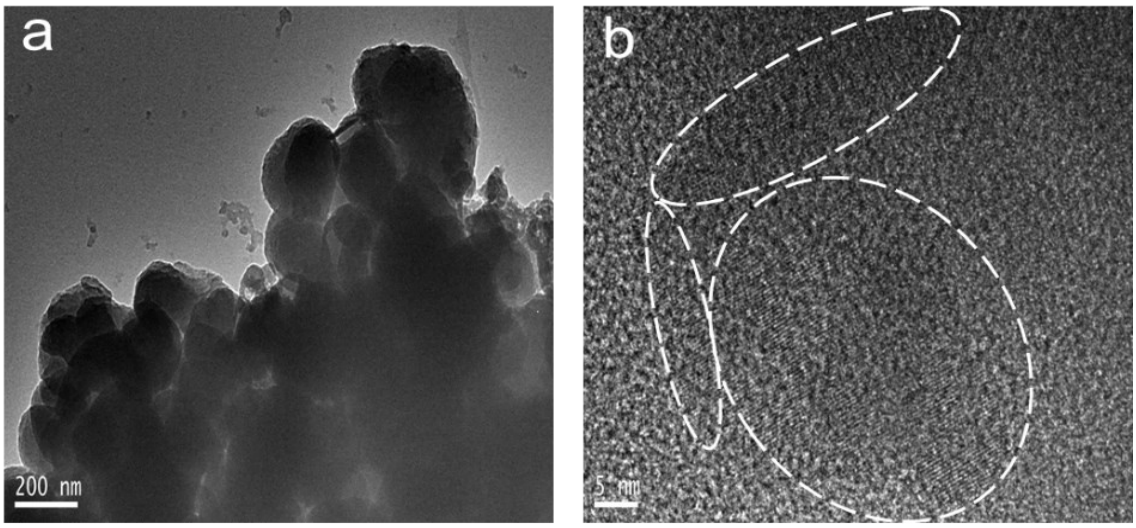

Figure S4. TEM and HRTEM images of ONCS-180.

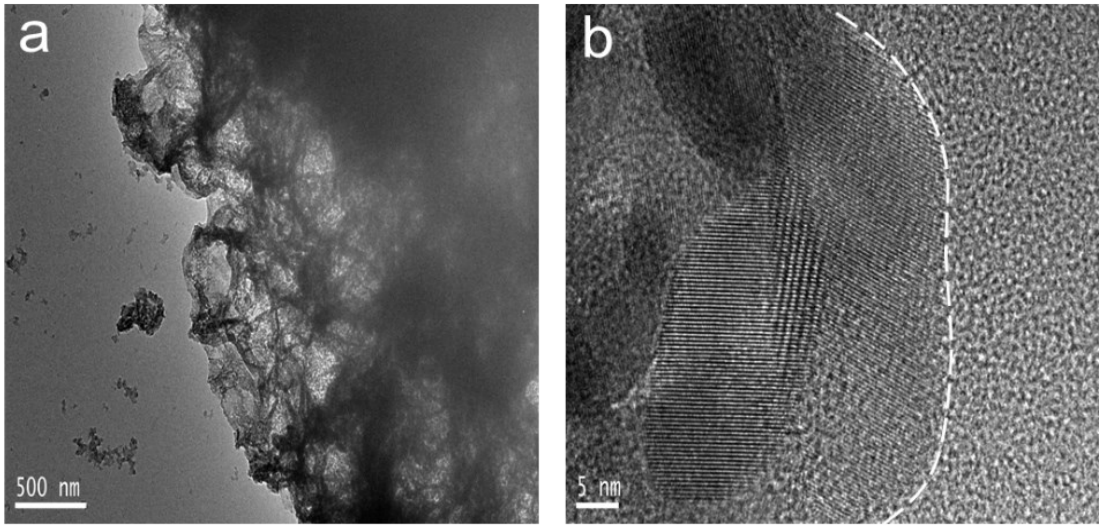

Figure S5. TEM and HRTEM images of ONCS-200.

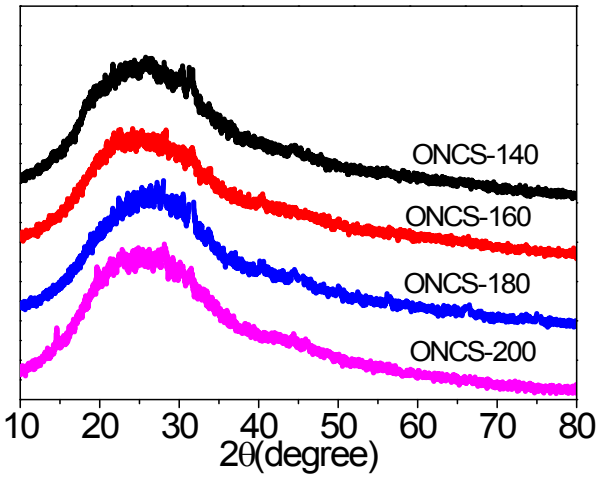

Figure S6. XRD patterns of all samples.

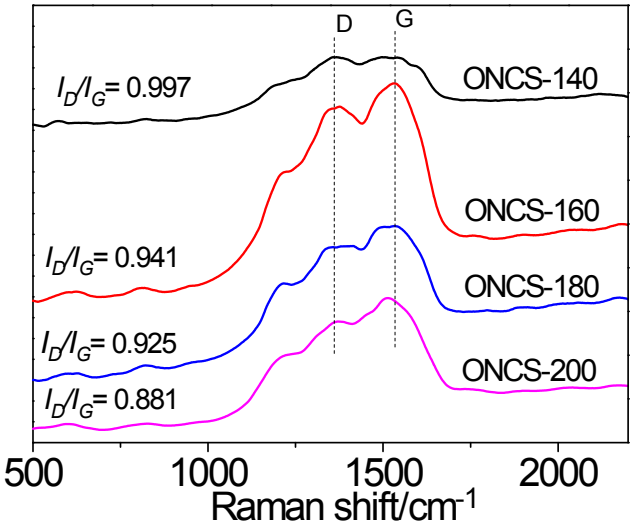

Figure S7. Raman spectra of all samples.

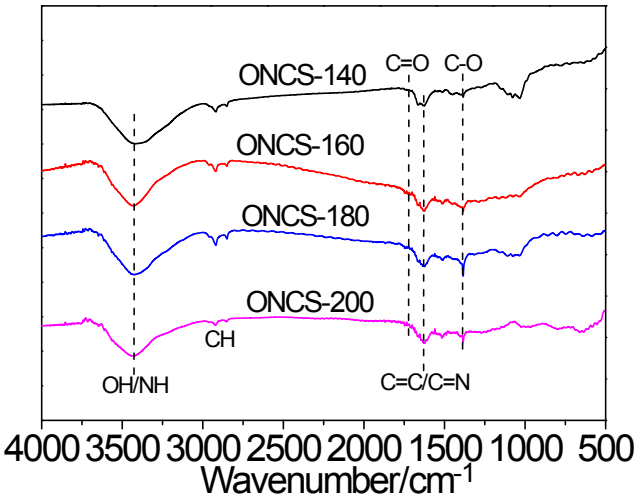

Figure S8. FTIR spectra of all samples.

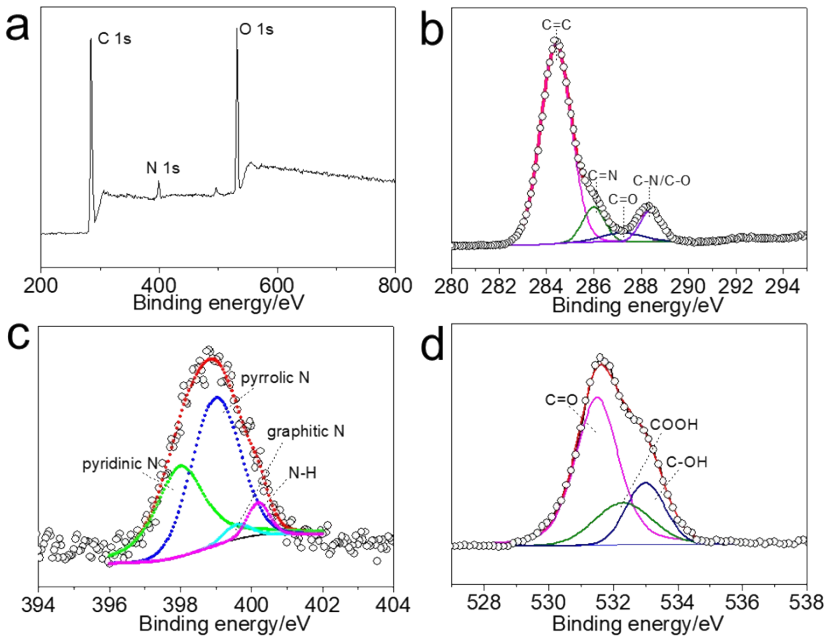

Figure S9. (a) XPS survey spectrum, (b) C1s spectrum, (c) N1s spectrum and (d) O1s spectrum of ONCS-160.

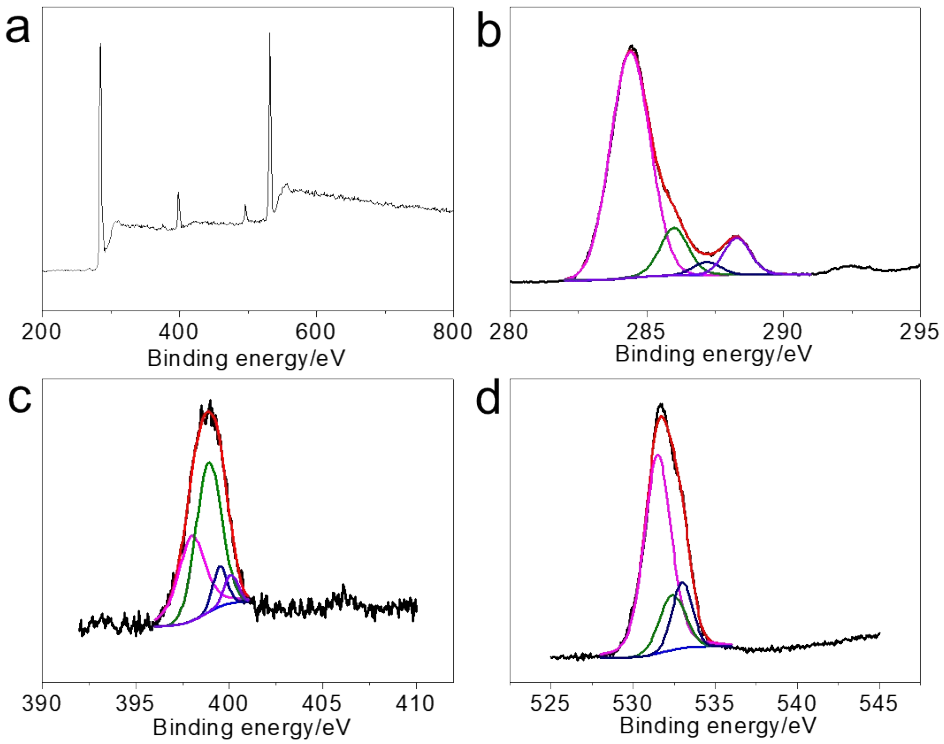

Figure S10. (a) XPS survey spectrum, (b) C1s spectrum, (c) N1s spectrum and (d) O1s spectrum of ONCS-140.

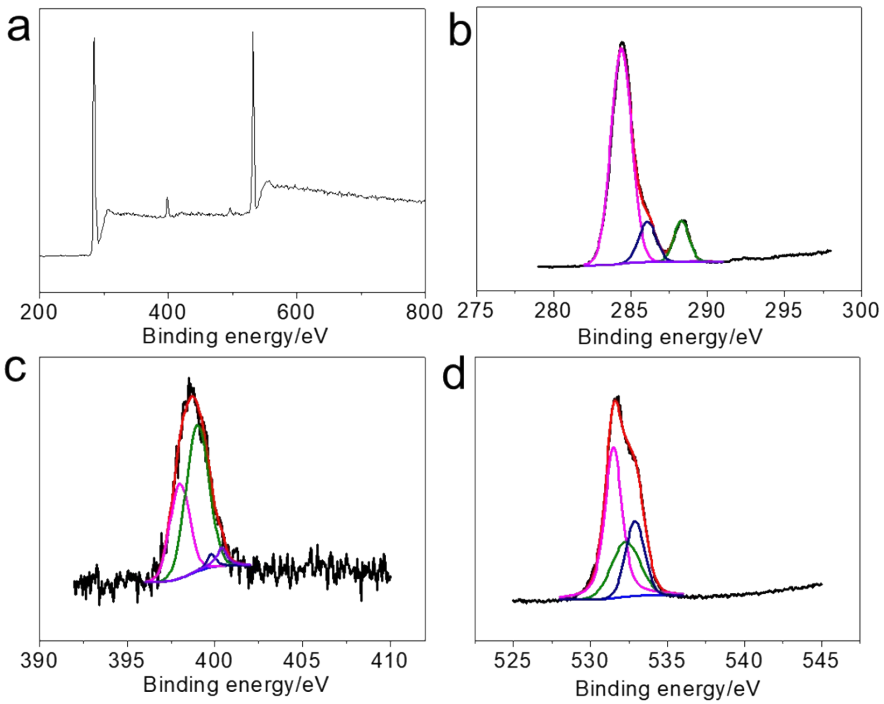

Figure S11. (a) XPS survey spectrum, (b) C1s spectrum, (c) N1s spectrum and (d) O1s spectrum of ONCS-180.

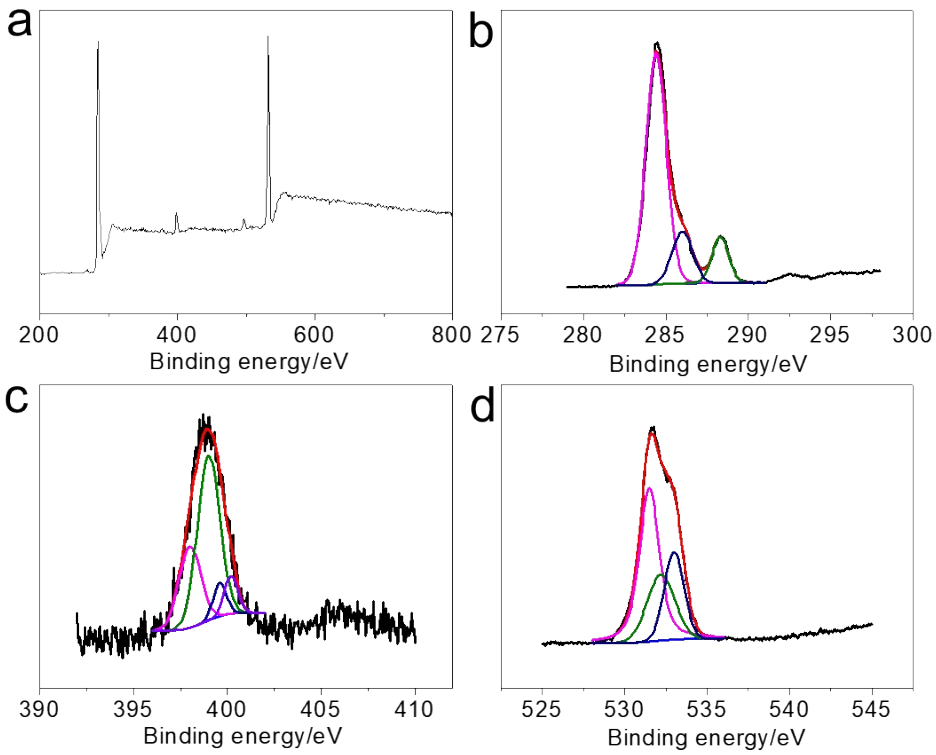

Figure S12. (a) XPS survey spectrum, (b) C1s spectrum, (c) N1s spectrum and (d) O1s spectrum of ONCS-200.

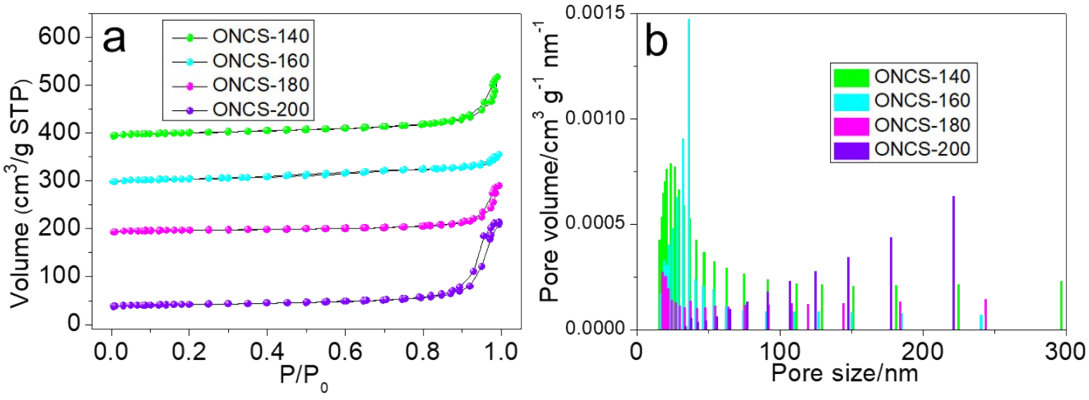

Figure S13. (a) N_2 adsorption/desorption isotherm, (b) size distribution of all samples.

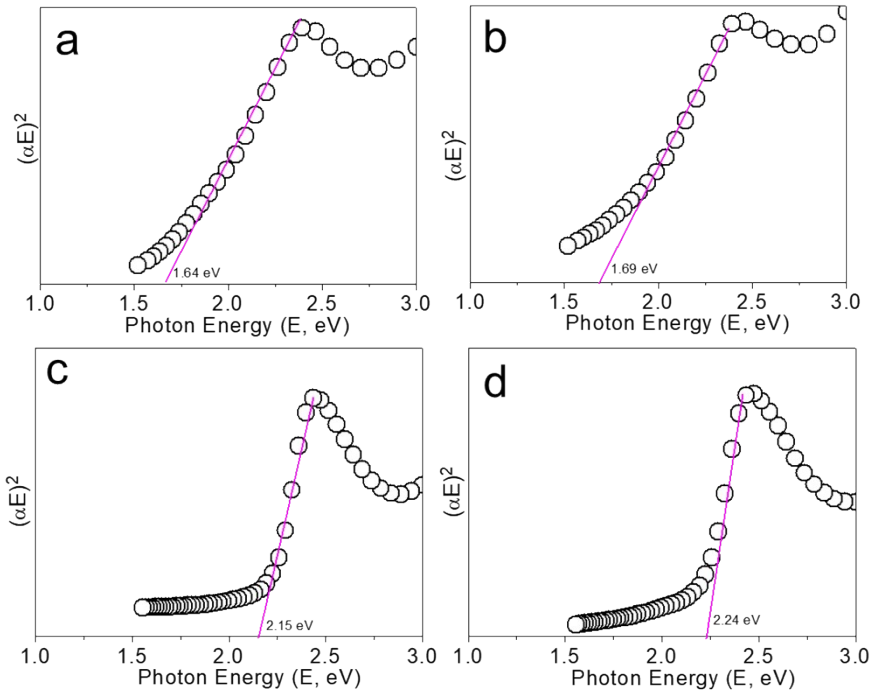

Figure S14. Band gaps of ONCS-140 (a), ONCS-160 (b), ONCS-180 (c) and ONCS-200 (d) samples determined by Tauc plots.

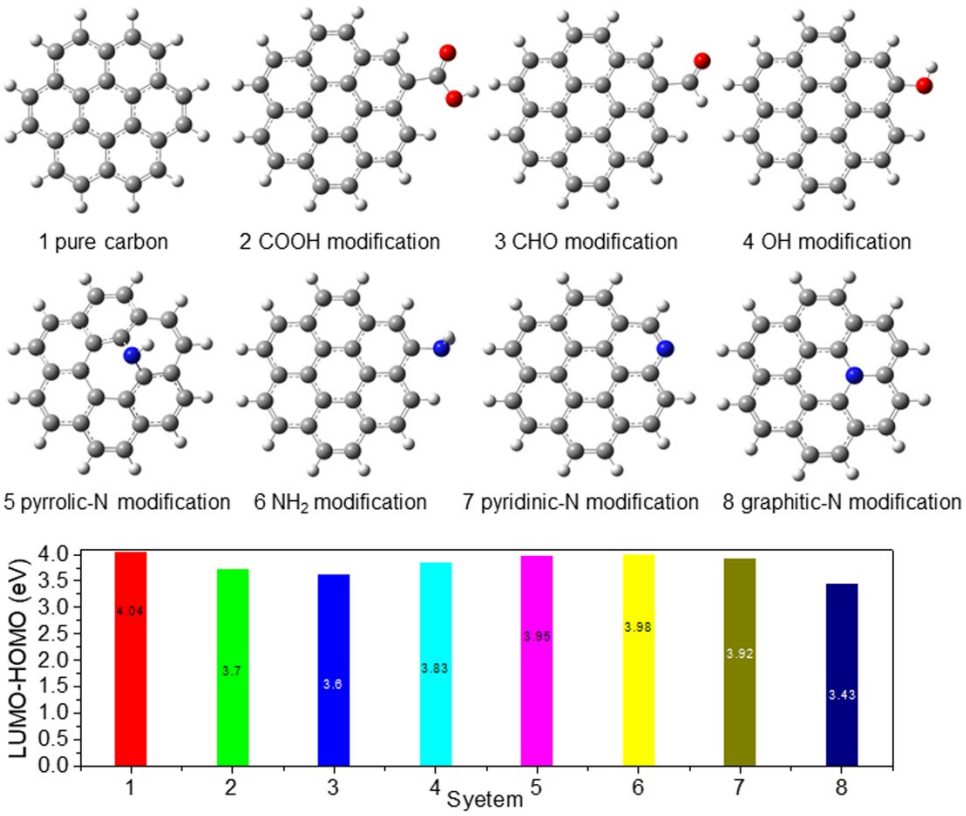

Figure S15. LUMO-HOMO values of different O- and N-modified carbons.

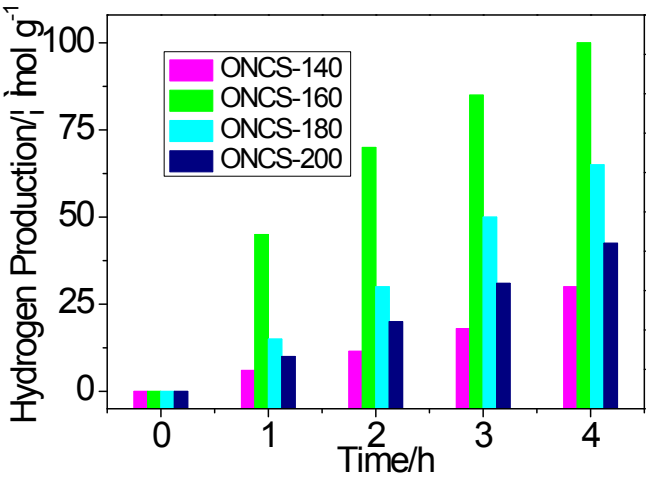

Figure S16. Photocatalytic mass activity of all samples.

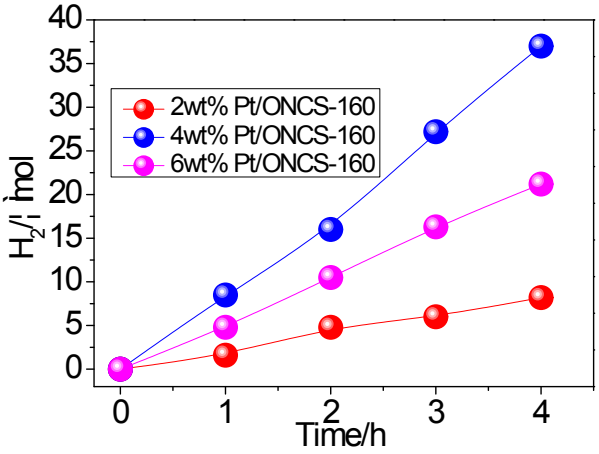

Figure S17. Photocatalytic activities of ONCS-160 with different Pt loading.

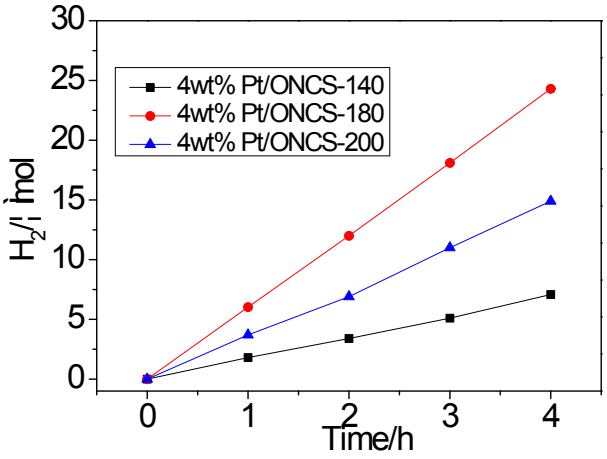

Figure S18. Photocatalytic activities of ONCS-140, ONCS-180 and ONCS-200.

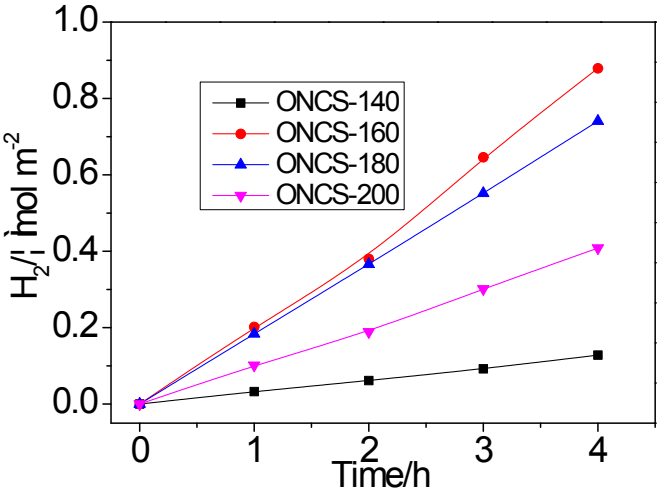

Figure S19. Photocatalytic specific activities of all samples (normalized by surface area).

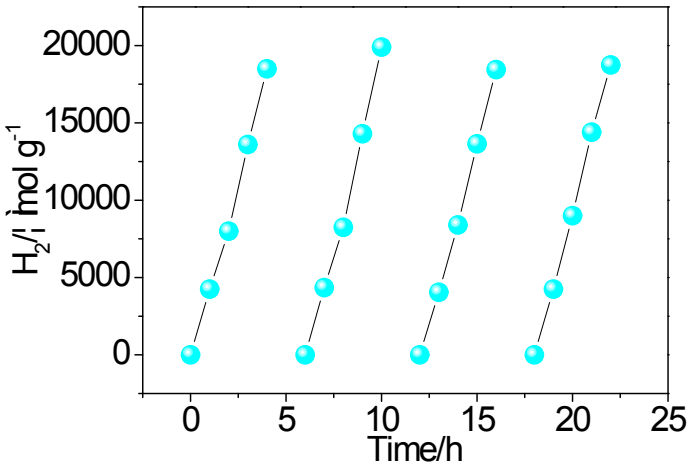

Figure S20. Mass activity of ONCS-160 during stability test under 530 nm irradiation.

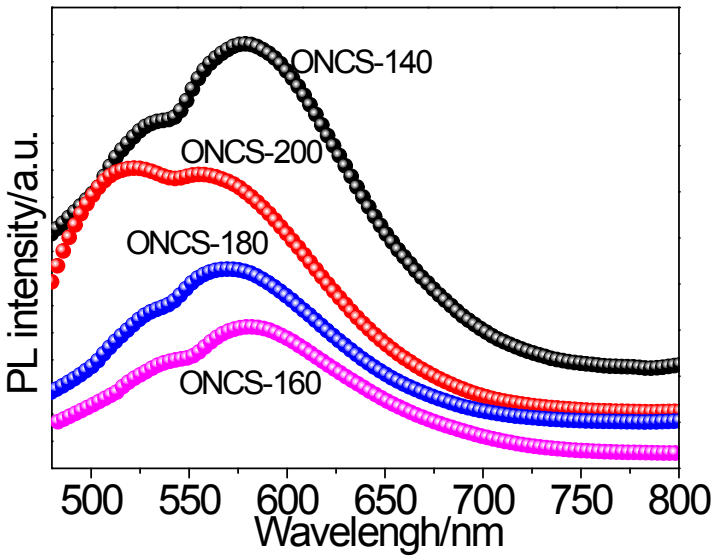

Figure S21. Steady-state PL spectra of all samples.

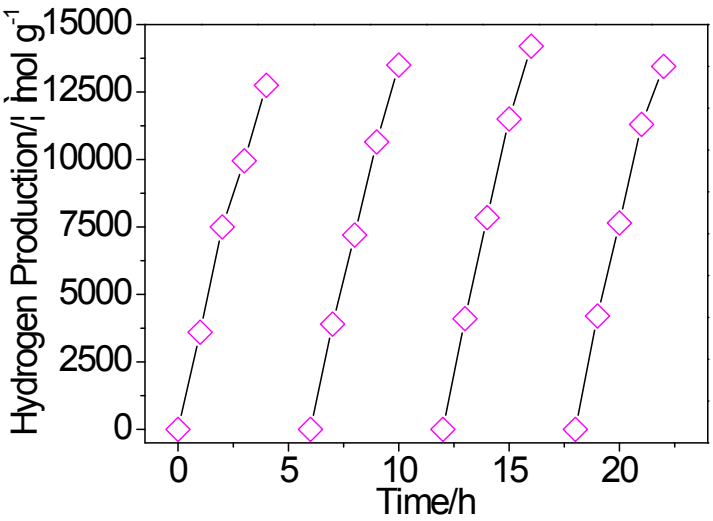

Figure S22. Mass activity of ONCS-160 during stability test under 660 nm irradiation.

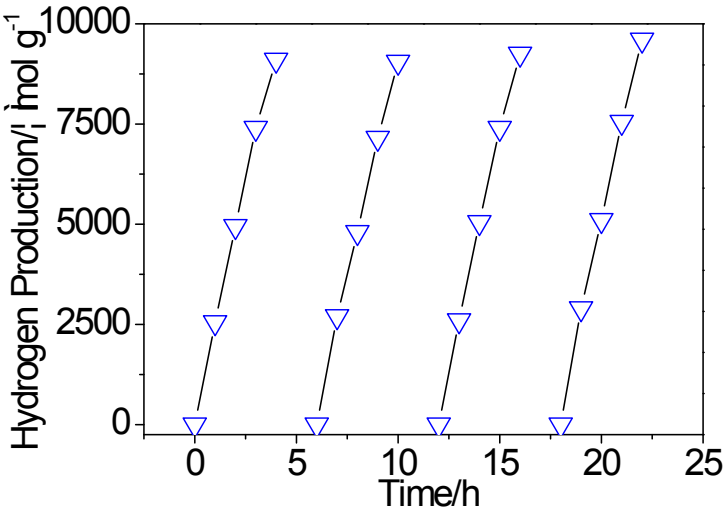

Figure S23. Mass activity of ONCS-160 during stability test under 730 nm irradiation.

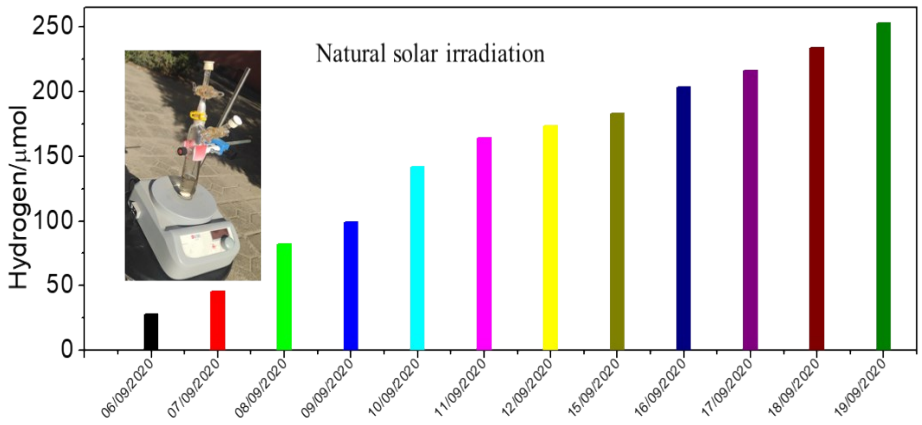

Figure S24. Hydrogen synthesis activity of ONCS-160 under natural solar irradiation.

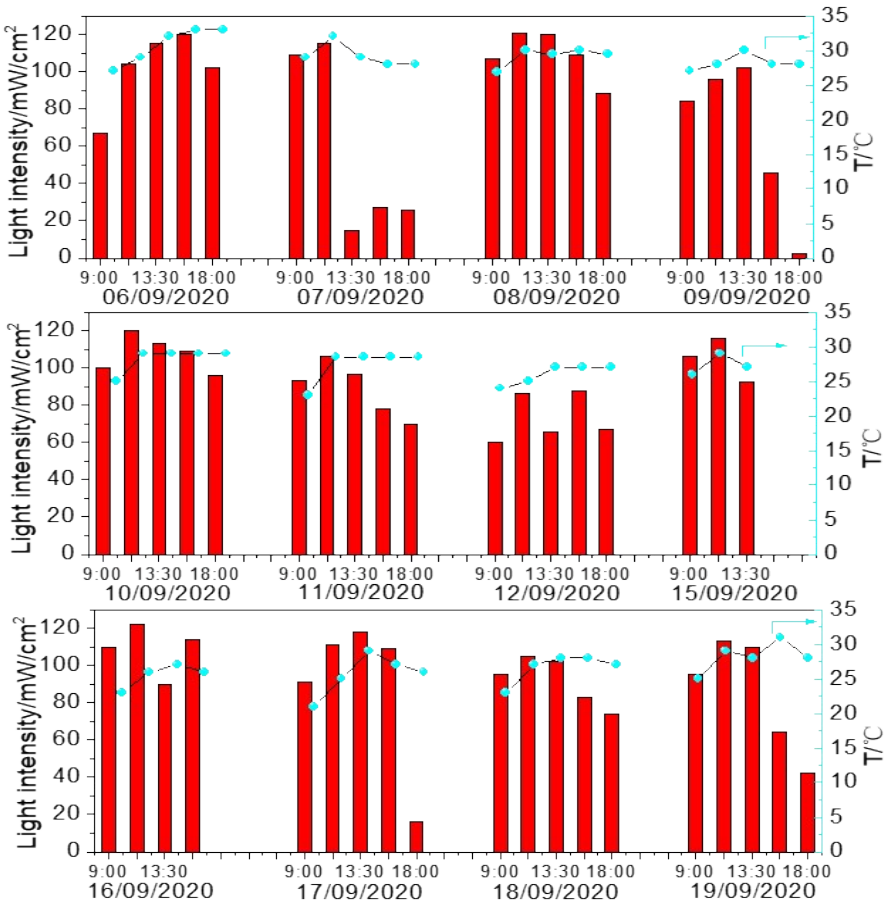

Figure S25. Sunlight intensity and ambient temperature (Taiyuan, China).

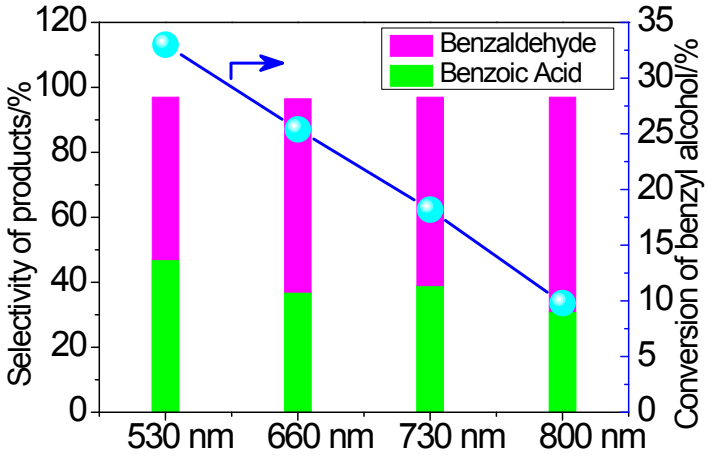

Figure S26. Benzyl alcohol oxidation activities of ONCS-160 under different irradiation wavelengths.

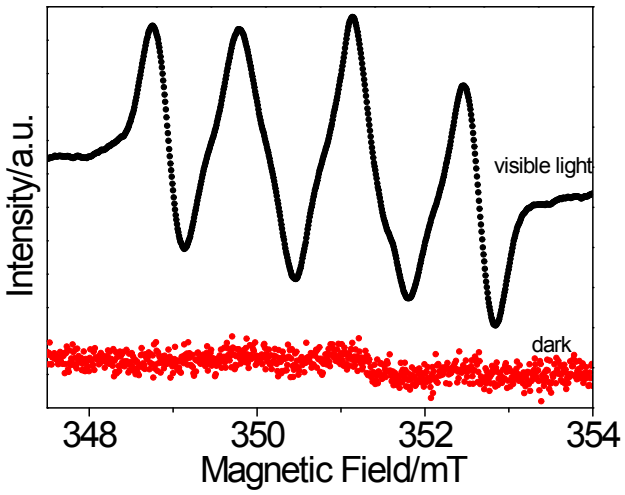

Figure S27. EPR spectra for DMPO-$O_2^{\bullet -}$ (α_H =1.03 mT, α_N = 1.38 mT).

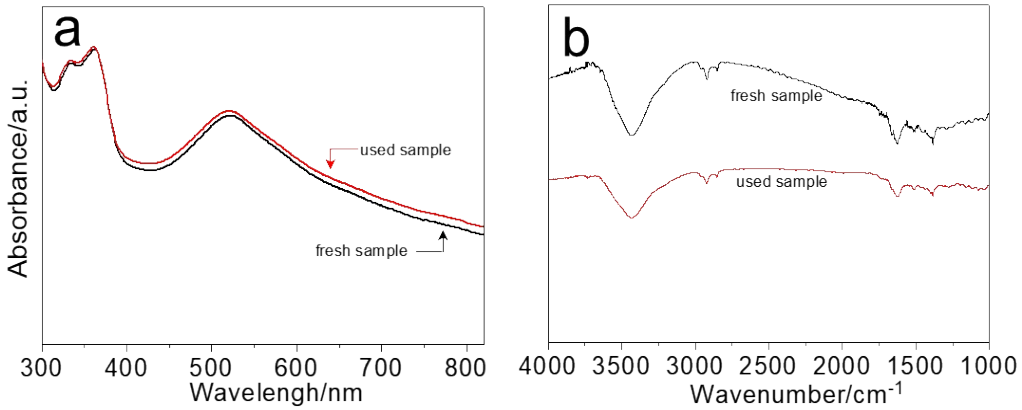

Figure S28. UV-vis absorption and FTIR spectra of fresh ONCS-160 and used ONCS-160 samples.

Table S1 Contents of C, N and O elements within ONCS samples.

Photocatalysts	C/at%	N/at%	O/at%
ONCS-140	68.1	5.8	26.1
ONCS-160	70.3	4.8	24.9
ONCS-180	73.3	4.7	22.0
ONCS-200	74.2	4.4	21.4

Table S2 Contents of C, N, O and H elements within ONCS samples determined by elemental analysis.

Catalysts	C/at%	N/at%	O/at%	H/at%
ONCS-140	62.4	3.2	20.5	13.9
ONCS-160	65.9	2.7	19.8	11.6
ONCS-180	70.3	2.4	18.2	9.1
ONCS-200	72.8	2.2	16.1	8.9

Table S3 Relative ratios of C=C, C=N, C=O and C-N/C-O groups determined from C 1s spectra of all samples.

Photocatalysts	C=C/%	C=N/%	C=O/%	C-N/C-O/%
ONCS-140	75.9	11.2	4.1	8.8
ONCS-160	76.3	10.7	3.6	9.4
ONCS-180	77.4	12.1	0	10.5
ONCS-200	77.9	10.5	0	11.6

Table S4 Relative ratios of pyridinic N, pyrrolic N, graphitic N and N-H groups of all samples determined from N 1s spectra.

Photocatalysts	pyridinic N/%	pyrrolic N/%	graphitic N/%	N-H/%
ONCS-140	36.3	50.7	7.7	5.3
ONCS-160	40.5	51.5	2.8	5.2
ONCS-180	33.6	58.9	2.7	4.8
ONCS-200	27.7	57.4	6.9	8.0

Table S5 Relative ratios of C=O, COOH and C-OH groups of all samples determined from O 1s spectra.

Photocatalysts	C=O/%	COOH/%	C-OH/%
ONCS-140	68.5	16.4	15.1
ONCS-160	60.8	19.6	19.6
ONCS-180	51.8	25.3	22.9
ONCS-200	51.6	24.9	23.5

Table S6 Electrical Properties of ONCS-160 and ONCS-200 samples.

Samples	Resistivity (Ω•cm)	Hall coefficients(cm^3/C)	Carrier concentration($/cm^3$)	Mobility ($cm^2/V•s$)
ONCS-160	8.69E+03	-2.51E+04	1.38E+11	5.19E+01
ONCS-200	2.49E+03	-9.87E+03	6.33E+11	3.97E+01

Table S7 LUMO and HOMO values of different O- and N-modified carbon.

System	HOMO (eV)	LUMO (eV)	bandgap(eV)
Pure carbon	-5.450508	-1.412981	4.04
COOH modification	-5.613671	-1.908950	3.70
CHO modification	-5.708380	-2.103565	3.60
OH modification	-5.232916	-1.399067	3.83
pyrrolic-N modification	-5.362897	-1.407919	3.95
NH_2 modification	-5.357343	-1.376244	3.98
pyridinic-N modification	-5.635689	-1.714182	3.92
graphitic-N modification	-9.212539	-5.782100	3.43

Table S8 Comparison of hydrogen photosynthesis activities with state-of-the-art photocatalysts under red/NIR light irradiation.

Photocatalysts	Solvents	Wavelength/ nm	H_2/ μmol h^{-1} g^{-1}	Quantum yield/%	Ref.
$W_{18}O_{49}$/g-C_3N_4	TEOA/Water	>700	0.034	0.016(800nm)	1
				0.013(700nm)	
				0.004(600nm)	
WO_2-Na_xWO_3	Phosphate/Water	980	10		2
BP-Au/$La_2Ti_2O_7$	Methanol/Water	>780	3		3
$ZnGeP_2$	Methanol/Water	> 800	0.77	0.18(850nm)	4
				0.4(600nm)	
Amorphous TiO_2	Methanol/Water	>750	32.48		5
NYFG/C_3N_4	TEA/Water	>980	103.87	0.8(980nm)	6
				0.2(800nm)	
				0.25(600nm)	
Au/g-C_3N_4	TEOA/Water	> 800	63.1		7
g-C_3N_4-Co-K	TEOA/Water	> 700	470		8
MoS_2-BP/GO	Methanol/Water	> 800	8.67		9
S/P	TEOA/Water	> 780	9.6	0.12(700 nm)	10
				0.25(600nm)	
Au-TiO_2-Pd	Methanol/Water	> 780	0.3		11
$Ni_3(C_3N_3S_3)$	TEOA/Water	> 800	0.004		12
g-C_3N_4/UFR-NC	TEOA/Water	> 780	0.016		13
Au/Pd-TiO_2	TEOA/Water	> 780	0.52		14
ONCS-160	Fomic acid/Water	660	3187.5	1.72(660nm)	this
		730	2275	0.89(730nm)	work
		800	680	0.52(800nm)	

BP=black phosphorous; NYFG = NaYF4:Yb,Tm,Gd; GO = graphene oxide; TEOA = triethanolamine; TEA = triethylamine; UFR-NC = formaldehyde resin-carbonized nitrogen doped carbon; CN-GP = graphited carbon ring domain

Table S9 Summary of average light intensity, average temperature and produced hydrogen under natural solar irradiation.

Date	Reaction time (h)	Average light intensity (mW/cm^2)	Average temperature (^oC)	Hydrogen (μmol)
2020.9.6	9.0	101.6	31.0	27.9
2020.9.7	7.0	66.5	29.2	17.3
2020.9.8	9.5	109.1	29.1	36.8
2020.9.9	8.0	82.0	28.2	16.8
2020.9.10	9.5	107.6	28.2	42.7
2020.9.11	8.0	93.5	27.4	22.4
2020.9.12	8.5	73.4	26.0	9.4
2020.9.15	4.5	104.8	27.3	9.5
2020.9.16	8.0	109.0	25.5	20.8
2020.9.17	8.0	89.1	25.6	12.8
2020.9.18	8.0	91.8	26.7	17.9
2020.9.19	8.0	85.3	28.2	18.9

Refences.

1. Zhang, Z.; Huang, J.; Fang, Y.; Zhang, M.; Liu, K.; Dong, B., A Nonmetal Plasmonic Z-Scheme Photocatalyst with UV- to NIR-Driven Photocatalytic Protons Reduction. *Adv. Mater.* **2017,** *29* (18), 1606688.

2. Cui, G.; Wang, W.; Ma, M.; Xie, J.; Shi, X.; Deng, N.; Xin, J.; Tang, B., IR-Driven Photocatalytic Water Splitting with WO_2-Na_xWO_3 Hybrid Conductor Materiasl. *Nano Lett.* **2015,** *15* (11), 7199-203.

3. Zhu, M.; Cai, X.; Fujitsuka, M.; Zhang, J.; Majima, T., Au/$La_2Ti_2O_7$ Nanostructures Sensitized with Black Phosphorus for Plasmon-Enhanced Photocatalytic Hydrogen Production in Visible and Near-Infrared Light. *Angew. Chem. Int. Ed.* **2017,** *56* (8), 2064-2068.

4. Li, X.; Wang, P.; Wu, Y.-Q.; Liu, Z.-H.; Zhang, Q.-Q.; Zhang, T.-T.; Wang, Z.-Y.; Liu, Y.-Y.; Zheng, Z.-K.; Huang, B.-B., $ZnGeP_2$: A near-infrared-activated photocatalyst for hydrogen production. *Front. Phys.* **2020,** *15* (2), 23604.

5. Jiang, J.; Tang, X.; Zhou, S.; Ding, J.; Zhou, H.; Zhang, F.; Zhang, D.; Fan, T., Synthesis of visible and near infrared light sensitive amorphous titania for photocatalytic hydrogen evolution. *Green Chem.* **2016,** *18* (7), 2056-2062.

6. Zhu, Y.; Zheng, X.; Lu, Y.; Yang, X.; Kheradmand, A.; Jiang, Y., Efficient upconverting carbon nitride nanotubes for near-infrared-driven photocatalytic hydrogen production. *Nanoscale* **2019,** *11* (42), 20274-20283.

7. Tian, H.; Liu, X.; Liang, Z.; Qiu, P.; Qian, X.; Cui, H.; Tian, J., Gold nanorods/g-C_3N_4 heterostructures for plasmon-enhanced photocatalytic H_2 evolution in visible and near-infrared light. *J. Colloid Interface Sci.* **2019,** *557*, 700-708.

8. Xue, Y.; Lu, S.; Liang, Z.; Guo, Y.; Cui, H.; Tian, J., Porous graphitic carbon nitride with nitrogen defects and cobalt-nitrogen (CoN) bonds for efficient broad spectrum (visible and near-infrared) photocatalytic H_2 production. *J. Colloid Interface Sci.* **2020**, *561*, 719-729.

9. Zhu, M.; Fujitsuka, M.; Zeng, L.; Liu, M.; Majima, T., Dual function of graphene oxide for assisted exfoliation of black phosphorus and electron shuttle in promoting visible and near-infrared photocatalytic H_2 evolution. *Appl. Catal. B Environ.* **2019,** *256,* 117864.

10. Cao, Q.; Guo, M.; Cao, J.; Lin, H.; Chen, Y.; Chen, S., An elemental S/P photocatalyst for hydrogen evolution from water under visible to near-infrared light irradiation. *Chem. Commun.* **2019,** *55* (87), 13160-13163.

11. Jiang, W.; Bai, S.; Wang, L.; Wang, X.; Yang, L.; Li, Y.; Liu, D.; Wang, X.; Li, Z.; Jiang, J.; Xiong, Y., Integration of Multiple Plasmonic and Co-Catalyst Nanostructures on TiO_2 Nanosheets for Visible-Near-Infrared Photocatalytic Hydrogen Evolution. *Small* **2016,** *12* (12), 1640-8.

12. Guo, F.; Shi, W.; Guo, S.; Guan, W.; Liu, Y.; Huang, H.; Liu, Y.; Kang, Z., $Ni_3(C_3N_3S_3)_2$ coordination polymer as a novel broad spectrum-driven photocatalyst for water splitting into hydrogen. *Appl. Catal. B Environ.* **2017,** *210*, 205-211.

13. Che, H.; Che, G.; Zhou, P.; Liu, C.; Dong, H.; Li, C.; Song, N.; Li, C., Nitrogen doped carbon ribbons modified g-C_3N_4 for markedly enhanced photocatalytic H_2-production in visible to near-infrared region. *Chem. Eng. J.* **2020,** *382*, 122870.

14. Cai, X.; Chen, Q.; Wang, R.; Wang, A.; Wang, J.; Zhong, S.; Liu, Y.; Chen, J.; Bai, S., Integration of Plasmonic Metal and Cocatalyst: An Efficient Strategy for Boosting the Visible and Broad-Spectrum Photocatalytic H_2 Evolution. *Adv. Mater. Interfaces* **2019,** *6* (17), 1900775.